Clays and Clay Minerals, Vol. 48, No. 4, 439–445, 2000.

QUANTITATIVE MEASUREMENT OF PARAMAGNETIC Fe^{3+} IN KAOLINITE

ETIENNE BALAN,[1] THIERRY ALLARD,[1] BRUNO BOIZOT,[1] GUILLAUME MORIN,[1] AND JEAN-PIERRE MULLER[1,2]

[1] Laboratoire de Minéralogie-Cristallographie, UMR 7590, CNRS, Universités Paris 6 et 7 and IPGP, Case 115, 4 Place Jussieu, 75252 Paris cedex 05, France

[2] Institut de Recherche pour le Développement (IRD), 213 rue Lafayette, 75480 Paris cedex 10, France

Abstract—A method is proposed to measure the absolute concentration of paramagnetic Fe^{3+} ions in kaolinite from various geochemical environments using powder X-band electron paramagnetic resonance (EPR) data. An Fe^{3+}-doped corundum sample is used as a concentration standard. The Fe^{3+} signal is calibrated by calculating the powder EPR spectra of Fe^{3+} ions in corundum and low-defect kaolinite. The paramagnetic Fe^{3+} concentration in other samples is obtained by an extrapolation procedure. This study provides a direct assessment of the iron distribution between isolated structural Fe^{3+} ions and other iron species, such as Fe^{3+} concentrated phases and Fe^{2+} ions. The concentration of isolated structural Fe^{3+} ranges between 200–3000 ppm and represents less than half of the total iron within kaolinite crystals.

Key Words—Electron Paramagnetic Resonance, EPR, Fe^{3+}, Kaolinite.

INTRODUCTION

Kaolinite is known to contain minor quantities of transition elements such as iron, vanadium, and manganese. The valence state of the ion and atomic position in the structure depend on the conditions of formation of the mineral (Muller and Calas, 1993; Muller *et al.,* 1995). Iron is the major impurity in kaolinite, and its concentration correlates with several macroscopic properties, such as the defect concentration and particle size (Cases *et al.,* 1982; Brindley *et al.,* 1986; Giese, 1988).

Studies (*e.g.,* Bonnin *et al.,* 1982; Schroeder and Pruett, 1996) have suggested that the distribution of trivalent iron in kaolinite may be determined spectroscopically. Electron paramagnetic resonance spectroscopy (EPR) distinguishes two forms of trivalent iron: (1) isolated Fe^{3+} ions isomorphously substituted for Al^{3+} within the kaolinite structure, herein referred to as "dilute" structural Fe^{3+}, and (2) poorly understood domains in which Fe^{3+} ions reside in close proximity (a few Å typically) to one another (*e.g.,* Hall, 1980; Bonnin *et al.,* 1982; Muller and Calas, 1993; Goodman and Hall, 1994). Fe^{3+} occurring in these domains is referred to as "concentrated" Fe^{3+}. Dilute structural Fe^{3+} exhibits a paramagnetic signal at low magnetic field. This signal is characterized by sharp EPR lines whose intensity increases with decreasing temperature. Nanometric domains of concentrated Fe^{3+} ions exhibit superparamagnetic or antiferromagnetic character. This is characterized by a broad line at high magnetic field, the intensity of which decreases with decreasing temperature. Diffuse reflectance spectroscopy (DRS) suggests that iron oxide or oxy-hydroxide nanophases may be responsible for this latter EPR response (Malengreau *et al.,* 1994). Magic-angle spinning nuclear magnetic resonance studies by Schroeder and Pruett (1996) and Schroeder *et al.* (1998) also suggested that the ordering pattern of Fe^{3+} between "dilute-Fe" and "clustered-Fe" may vary between different kaolinite samples.

Although the occurrence of different modes of iron incorporation within kaolinite crystals is well established, the Fe^{3+} distribution among these forms in natural kaolinites has not been quantitatively determined. The present study determines a quantitative approach to measure dilute structural Fe^{3+} by combining calculation of X-band EPR spectra (Balan *et al.,* 1999; Morin and Bonnin, 1999) with data from an Fe^{3+}-doped α-Al_2O_3 standard.

MATERIALS AND EXPERIMENTAL

Samples

Kaolinite. Twelve kaolinite samples (Table 1) were selected from various geochemical environments, including hydrothermal deposits, sediments, and soils. Non-kaolin group minerals present in small quantities are muscovite, illite, quartz, and Al, Fe, or Ti oxides or hydroxides. Grain-size separation (Table 1) was used to remove most of these ancillary phases and to produce homogeneous samples. Accessible iron oxides were removed using the complexing dithionite-citrate-bicarbonate (DCB) method (Mehra and Jackson, 1960). This treatment has no apparent effect either on the kaolinite structure or on the shape and intensity of the EPR signal of Fe^{3+} (Muller and Calas, 1989). The remaining iron concentration, measured by inductively coupled plasma atomic emission spectrometry at the Centre de Recherches Pétrographiques et Géochimiques (CRPG, Nancy, France), was <1 wt. % and varied between 1800–7700 ppm ([Fe]chem, Table 1).

Table 1. Characterization of the kaolinites.

Sample	Reference	Origin	Anc. miner.	$[Fe]_{chem}$	% Fe^{2+}	$[Fe^{3+}]_{EPR}$	R2[7]
DCV >2 μm	Gaite *et al.* (1993)	Aveyron[1] (France)	—	2190	31[6]	900	1.35
GB1	Cases *et al.* (1982)	Cornwall[1] (GB)	M, Q	3500	nd	750	1.13
GB3	Cases *et al.* (1982)	Cornwall[1] (GB)	M, Q	4650	43[5]	1700	1.09
KGa-1	van Olphen and Fripiat (1979)	Georgia[2] (USA)	A	1840	50[4]	450	1.03
KGa-2	van Olphen and Fripiat (1979)	Georgia[2] (USA)	A	7720	nd	3000	0.69
PDP3 <38 μm	Delineau *et al.* (1994)	Charentes[2] (France)	G	2020	nd	300	0.90
CHA2 <5 μm	Delineau *et al.* (1994)	Charentes[2] (France)	I, Q	6140	nd	1250	0.52
FBT2 <38 μm	Delineau *et al.* (1994)	Charentes[2] (France)	Q, A	7280	nd	1250	0.44
FU7	Cases *et al.* (1982)	Charentes[2] (France)	Q, A	6930	25[5]	1050	0.23
A1 <20 μm	Lucas *et al.* (1987)	Manaus[2] (Brasil)	—	5460	nd	2800	0.70
B4 <20 μm	Lucas *et al.* (1987)	Manaus[3] (Brasil)	G, A	4790	nd	2800	0.23
GOY <0.5 μm	Muller and Bocquier (1987)	Goyoum[3] (Cameroon)	—	nd	nd	2200	0.49

[1] Hydrothermal.
[2] Sediment.
[3] Soil.
[4] Murad and Wagner (1991).
[5] Bonnin *et al.* (1982).
[6] Delineau (1994).
[7] R2 : XRD disorder index from Liétard (Cases *et al.*, 1982; Gaite *et al.*, 1993). Ancillary minerals: Q: quartz; A: anatase; I: illite; M: mica; G: gibbsite. $[Fe]_{chem}$: iron concentration in ppm measured on samples with Fe-oxides removed by DCB methods. % Fe^{2+}: divalent iron concentration expressed as a percentage of the total iron concentration. $[Fe^{3+}]_{EPR}$: trivalent iron concentration expressed in ppm.

The kaolinite concentration of the samples varied from ~85% (sample GB3) to near 100% (sample DCV). Most of these samples were recently studied by examining the shape of the Fe^{3+} EPR signal and the defect nature of the kaolinite (Gaite *et al.*, 1993, 1997; Balan *et al.*, 1999).

Standard. Kaolinite cannot be used as a standard for concentration measurement of dilute Fe^{3+} because samples always appear to contain concentrated Fe phases, including iron oxide or oxy-hydroxide nano-phases resistant to DCB treatment (Malengreau *et al.*, 1994). EPR spectra of synthetic iron-doped kaolinites exhibit a broad superparamagnetic signal arising from concentrated iron phases (Petit and Decarreau, 1990). It is thus not possible to obtain a kaolinite standard with a dilute structural Fe^{3+} content equal to the total iron content. In contrast, Fe-doped α-Al_2O_3 standards show a homogeneous distribution of Fe^{3+} below 1.25 mol % (De Biasi and Rodrigues, 1983).

Boizot (1996) reported that heating gibbsite for 1 wk at 1350°C destroys iron oxide nano-phases and produces diffusion of Fe^{3+} ions through the subsequently formed α-Al_2O_3 structure. The absence of concentrated Fe domains or Fe phases in the resulting iron-doped α-Al_2O_3 is indicated both by the lack of any detectable superparamagnetic absorbance in the spectra of the calcined corundum powders and by the linear correlation observed between the EPR intensity and the iron concentration (to 380 ppm). Therefore, a sample of α-Al_2O_3 prepared by Boizot (1996) containing 280 ppm Fe was used as a standard for dilute Fe^{3+} content. Discrepancies in EPR absorbance between α-Al_2O_3 and kaolinite owing to dielectric losses in the resonance cavity are limited because of their close dielectric constants (10.43 and 11.8, respectively; Olhoeft, 1981; Shannon and Rossman, 1992).

EPR spectroscopy

EPR measurements at 9.42 GHz (X-band) were performed at 120 K using a Bruker ESP300E spectrometer equipped with a nitrogen-flow device for cooling. Low-temperature recording enhances the EPR signal owing to dilute Fe^{3+} compared to the broad signal owing to concentrated Fe^{3+} (Bonnin *et al.*, 1982). Spectra were recorded with 40 mW microwave power. No saturation of the paramagnetic Fe^{3+} signal was observed with increasing power to 60 mW. Powder samples were placed in pure silica tubes (Suprasil grade). To ensure reliability of intensity measurements, the tubes were filled to constant volume such that the sample height was greater than the resonance cavity. All spectra were recorded using the same measurement parameters (frequency modulation = 100 kHz, amplitude modulation = 5 Gauss), whereas the gain depended on the sample. Spectra were then normalized with respect to gain and sample weight, which is proportional to sample density.

RESULTS AND DISCUSSION

The EPR absorbance of paramagnetic Fe^{3+} is proportional to the number of isolated Fe^{3+} ions within the resonance cavity. If spectra were recorded under the same experimental conditions, EPR spectra of the standard and each kaolinite can be compared to determine relative variations in dilute Fe^{3+} concentration (Calas, 1988; Weil *et al.*, 1994). However, because

https://doi.org/10.1346/CCMN.2000.0480404 Published online by Cambridge University Press

Fe^{3+} site symmetry between kaolinite and standard differ and site symmetry strongly modifies the EPR absorbance, a direct comparison between EPR absorbances cannot be made. By calculating the EPR spectra of kaolinite and the standard, this difficulty may be overcome. However, the fine-structure parameters, which describe the symmetry of the various Fe^{3+} sites, must be determined. Following this procedure, the concentration of dilute structural Fe^{3+} in a reference kaolinite sample is obtained by comparison to the standard. Then, the dilute structural Fe^{3+} concentration in other kaolinite samples is extrapolated from the concentration as determined in the reference kaolinite sample.

EPR spectra and fine-structure parameters for kaolinites and standard

Figure 1 shows the normalized X-band EPR spectra of four kaolinite samples recorded at 120 K in the 0.0–0.3 Tesla (T) range together with the X-band EPR spectrum of the Fe^{3+}-doped α-Al_2O_3 standard obtained at 120 K. These kaolinite EPR spectra show the variation in shape and intensity of the Fe^{3+} EPR signal commonly observed in natural kaolinites (Muller and Calas, 1993; Gaite *et al.*, 1997). The spectra show two superposed signals, classically referred to as $Fe_{(I)}$ and $Fe_{(II)}$, which are interpreted as two Fe^{3+} sites with different distortion (*e.g.*, Muller *et al.*, 1995). Determination of the corresponding fine-structure parameters (Gaite *et al.*, 1993; Balan *et al.*, 1999) showed that both $Fe_{(II)}$ and $Fe_{(I)}$ signals correspond to Fe^{3+} substituted for Al^{3+} within the dioctahedral sheet of the kaolinite structure. The $Fe_{(II)}$ signal corresponds to sites within low-defect kaolinite whereas the $Fe_{(I)}$ signal is produced by changes of the site symmetry owing to the random distribution of vacant octahedral sites in successive layers (Balan *et al.*, 1999). In the low-defect DCV sample, the $Fe_{(I)}$ signal includes the contribution of a minor amount of Fe^{3+} in low-defect dickite.

The powder EPR spectrum at 120 K of the dilute Fe^{3+} in α-Al_2O_3 differs significantly from those of kaolinites. The α-Al_2O_3 spectrum is similar to the room temperature spectra reported by De Biasi and Rodrigues (1983) and Morin and Bonnin (1999). However, weakly allowed transitions at low magnetic field are absent because the recording temperatures differ. The fine-structure parameters of the Fe^{3+} site in α-Al_2O_3 at 120 K were refined following the method of Morin and Bonnin (1999), which is based on a full-diagonalization of the spin Hamiltonian (B_2^0 = 0.0572 cm^{-1}; $60 \times B_4^0 = -0.0114$ cm^{-1}; $60 \times B_4^3$ = 0.2257 cm^{-1}, where B_2^0, B_4^0, and B_4^3 are the conventional fine-structure parameters for the trigonal symmetry of Fe^{3+} site in α-Al_2O_3). These parameters differ slightly from those refined at room temperature (Bogle and Symmons, 1959; Morin and Bonnin, 1999).

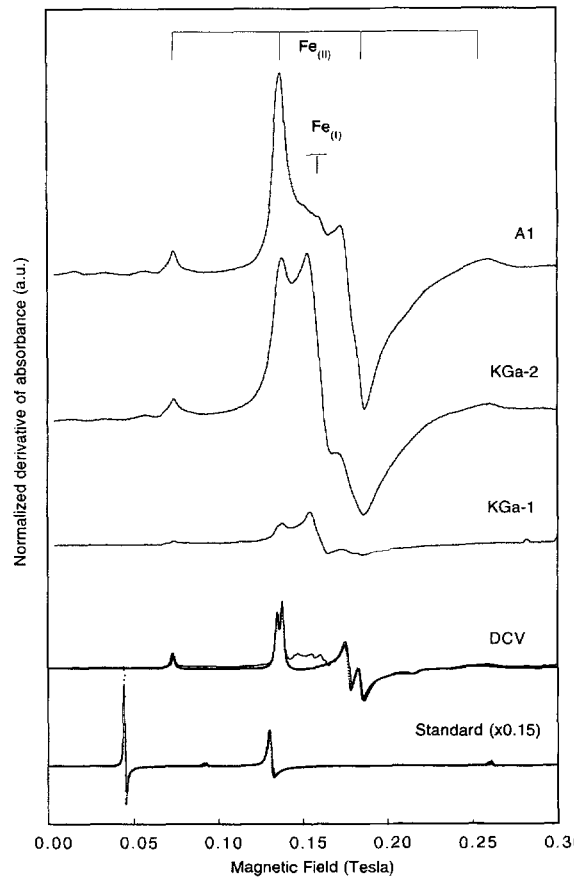

Figure 1. X-band EPR spectra normalized against gain and sample weight (see text) of four kaolinite samples (A1, KGa-1, KGa-2, and DCV) and standard (0.15×). Dotted lines represent the calculated spectra of the $Fe_{(II)}$ signal for DCV and for the standard. To establish a quantitative relation between the EPR absorbance of the standard and kaolinite, the spectra were calculated for the same quantity of Fe^{3+}. They were subsequently multiplied by a scale factor, S, to fit the experimental spectra (DCV_{calc}, S = 0.80; Standard, S = 0.36).

Calibration of the absorbance of dilute Fe^{3+} in kaolinite

Fe^{3+} in $Fe_{(II)}$ sites. Sample DCV was used for calibration of the absorbance of Fe^{3+} in $Fe_{(II)}$ sites because the corresponding fine-structure parameters of this sample were previously determined accurately (Balan *et al.*, 1999). EPR spectra of Fe^{3+} in $Fe_{(II)}$ sites of DCV and in α-Al_2O_3 were calculated with the ZFSFIT code (Morin and Bonnin, 1999), which models powder EPR spectra with anisotropic line-broadening effects. Both experimental spectra were adjusted (Figure 1) by fitting a scale factor, S, as a free parameter (S_{DCV} = 0.80; S_{std} = 0.36). Because the Fe^{3+} concentration in the standard is 280 ppm, a value of 620 ppm is determined for Fe^{3+} in DCV $Fe_{(II)}$ sites.

Derivation of total Fe^{3+} concentration. The calibration of the absorbance of Fe^{3+} in $Fe_{(I)}$ sites is not obtained

https://doi.org/10.1346/CCMN.2000.0480404 Published online by Cambridge University Press

directly because the accurate calculation of the $Fe_{(I)}$ signal in kaolinites is both difficult and time-consuming (Balan *et al.,* 1999). The most intense X-band EPR signal (Figure 2) owing to Fe^{3+} in both $Fe_{(I)}$ and $Fe_{(II)}$ sites occurs between 0.1–0.25 T (Figure 2a). This signal arises from the angular dependencies of the spin transition inside the central spin doublet. Each energy level is sorted in ascending order and labeled from 1 to 6 for convenience. This transition is thus referred to as the 34 transition (see Balan *et al.,* 1999). Thus, the double integration of this signal leads to the total dilute Fe^{3+} concentration, provided that the $Fe_{(I)}$ and $Fe_{(II)}$ sites contribute similarly to the 34 transition absorbance.

The $Fe_{(I)}$ signal actually corresponds to a site distribution ranging continuously between the Fe sites of low-defect kaolinite and those of low-defect dickite (Balan *et al.,* 1999). The theoretical integrated absorbance of the 34 transition was thus calculated for both sites and was found to be 10% higher for the dickite sites. Consequently, the integration of the EPR signal, including both $Fe_{(I)}$ and $Fe_{(II)}$ signals in the 34 transition range, leads to a maximum overestimation of ~10% of the Fe^{3+} concentration corresponding to the $Fe_{(I)}$ signal. Because the contribution of each site in the total spectrum is difficult to determine accurately, the discrepancy is included in the error range in the calculation (below) of the Fe^{3+} concentration.

Error range

The major systematic errors are attributed to the fitting of the Fe^{3+} spectra for the standard and the DCV sample. Note in Figure 1 that small discrepancies remain between experimental and calculated spectra. This is related to parameters not considered, such as anisotropic broadening of the Fe^{3+} lines of α-Al_2O_3 owing to slight fluctuations of the crystal field (Boizot, 1996; Morin and Bonnin, 1999). However, by comparison of calculated and experimental absorbance spectra (Figure 2c for DCV), the corresponding error is less than ±20%.

Non-systematic errors arise from experimental uncertainties and from the baseline extraction procedure. Repeated experiments showed that the uncertainty of the data is within ±10% (Allard *et al.,* 1994). Error related to baseline extraction is estimated at less than ±10%. Finally, overestimation of the paramagnetic Fe^{3+} concentration in the high-defect kaolinites, where the $Fe_{(I)}$ signal dominates, is <10%.

Consequently, the uncertainty on the absolute values of the paramagnetic Fe^{3+} concentration in kaolinite determined using the present method is assessed by convoluting the systematic error with the non-systematic errors. Assuming a Gaussian distribution for both error types, results are thus within ±35%.

Dilute structural Fe^{3+} content in studied kaolinite samples

DCV sample. Figure 2b presents the absorbance curves obtained from the first integration of the EPR spectra of Figure 2a. The absorbance curves are related to the superposition of the absorbances of the 34 and 12 transitions. The latter transition, which appears on the absorbance curve as a step at 0.07 T, corresponds to the transition inside the lowest spin doublet. Absorbance bands are superposed on a rising slope because of the presence of concentrated Fe phases resistant to DCB treatment. Absorbances relating to the 12 transition and concentrated Fe phases are considered as linear background (Figure 2b). Figure 2c shows absorbance curves of the 34 transition obtained by subtraction of this background.

The total concentration of dilute structural Fe^{3+} is deduced by comparing the absorbance curve areas. Because the area of the $Fe_{(II)}$ absorbance curve corresponds to 620 ppm of Fe^{3+}, the total concentration of dilute structural Fe^{3+} is ~900 ppm. This low Fe^{3+} concentration in DCV is consistent with the negligible contribution of dipolar magnetic broadening arising from limited interactions between dilute paramagnetic Fe^{3+} ions. Indeed, the 17 Gauss line-width of the 12 line at 0.07 T is consistent with the expected line-width from super-hyperfine interactions between the electronic spin of Fe^{3+} and the ^{27}Al nuclear spin (De Biasi and Rodrigues, 1983).

Other samples. Dilute structural Fe^{3+} concentrations (Table I, $[Fe^{3+}]_{EPR}$) for the other studied samples were determined by comparison with the DCV sample. Integrated signals obtained for samples A1, KGa-1, and KGa-2 are compared to DCV in Figure 3. The concentration determined by weight of dilute structural Fe^{3+} in the kaolinite samples is <3000 ppm (Figure 4). In each case, the $[Fe^{3+}]_{EPR}$ is less or equal to half of the total iron concentration. This indicates significant partitioning of iron in natural kaolinites.

In addition to dilute structural Fe^{3+}, three other forms of iron may account for the remaining part of

→

Figure 2. (a) Normalized X-band EPR spectrum of DCV and calculated $Fe_{(II)}$ spectrum showing the relationship of the main EPR signals to the angular dependencies of the 34 transition. (b) Comparison of the experimental and calculated absorbance of DCV showing the superposition of the 34 transition to a baseline owing to the 12 transition and to the broad superparamagnetic signal on the experimental absorbance. (c) Comparison of the experimental and calculated $Fe_{(II)}$ absorbance of the 34 transition after baseline correction. The ratio of the integrated areas allows for the determination of the paramagnetic structural Fe^{3+} concentration in DCV.

https://doi.org/10.1346/CCMN.2000.0480404 Published online by Cambridge University Press

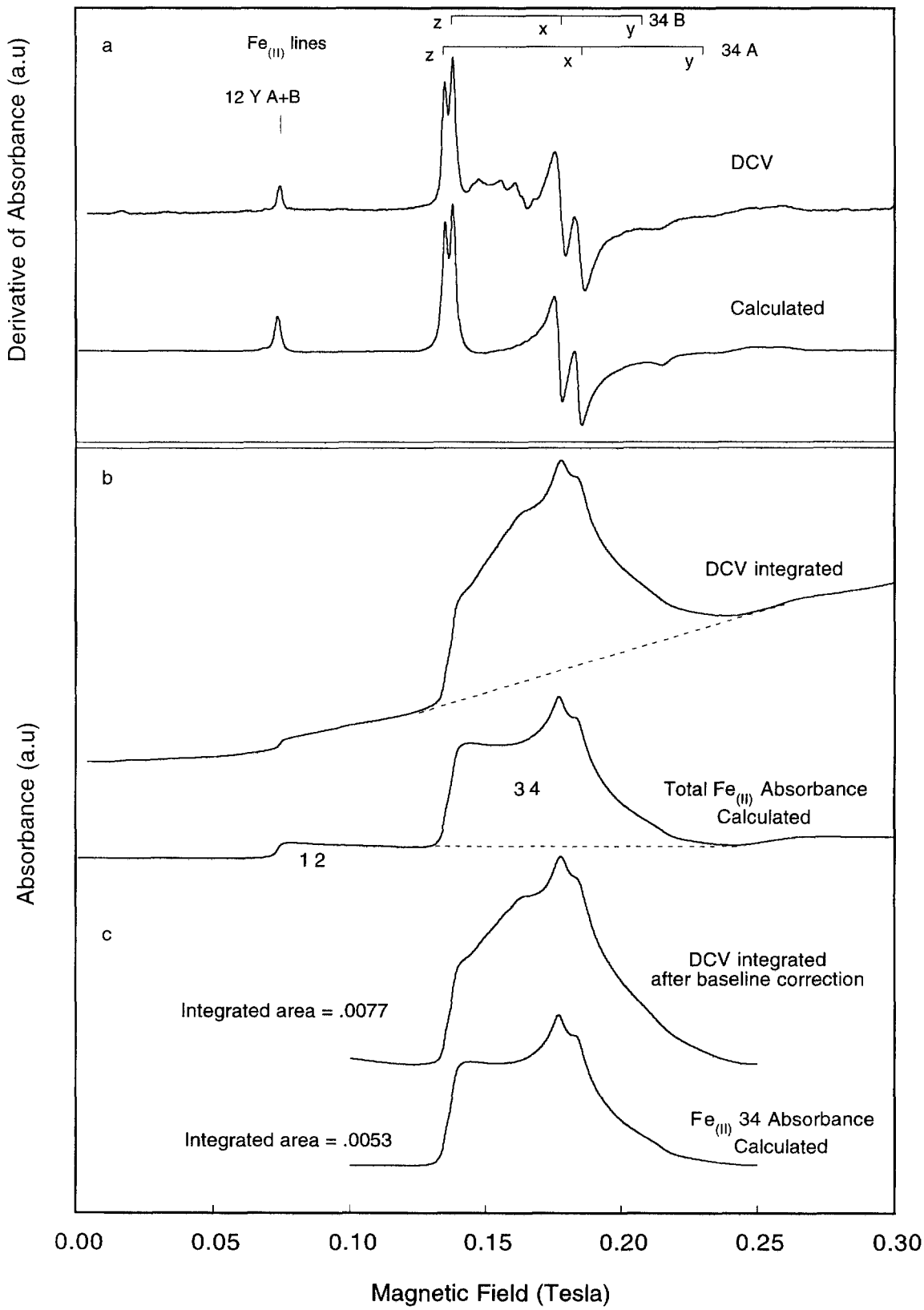

https://doi.org/10.1346/CCMN.2000.0480404 Published online by Cambridge University Press

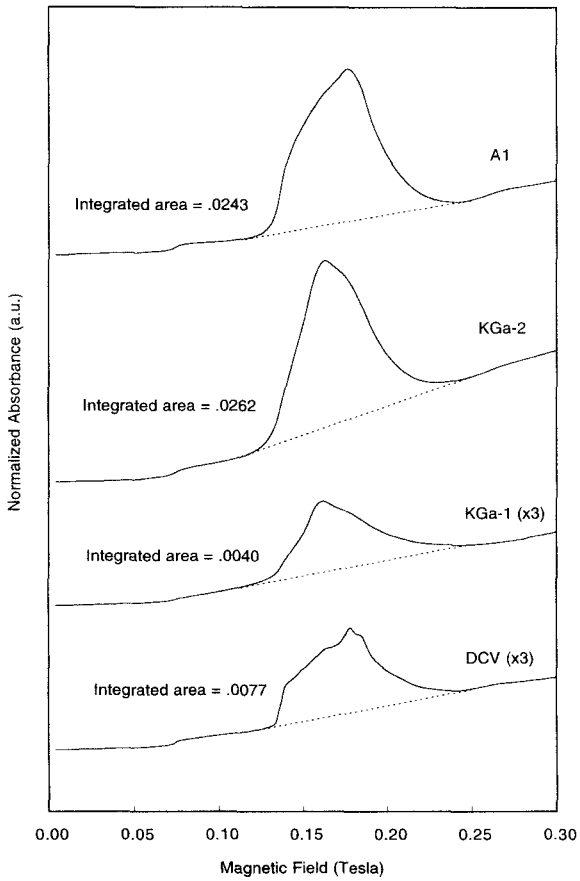

Figure 3. Comparison of experimental 34 absorbances of four kaolinite samples (A1, KGa-1, KGa-2, and DCV). The baseline owing to the 12 transition and to the broad superparamagnetic signal is approximated by the dotted line. The ratio of the integrated areas of A1, KGa-1, and KGa-2 to the DCV area allows the determination of the dilute structural Fe^{3+} concentration.

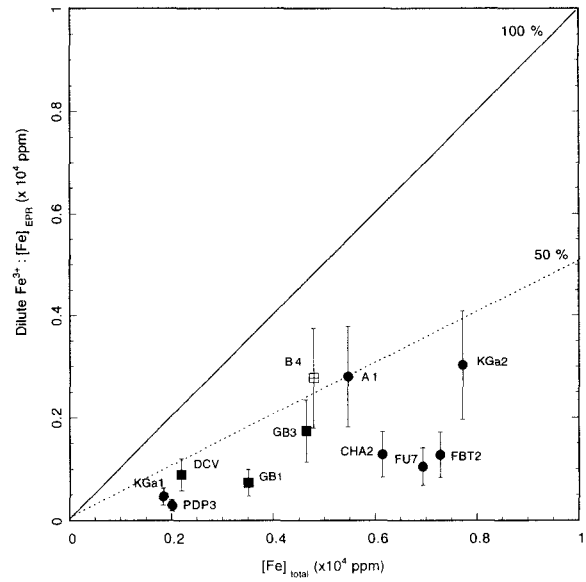

Figure 4. Dilute structural Fe^{3+} concentration plotted as a function of the total iron concentration determined by chemical analysis. Error bars represent ±35%, the estimated uncertainty. Note that the paramagnetic structural Fe^{3+} concentration is always lower than the total iron concentration.

iron in the natural kaolinites examined here: Fe^{2+} ions, clusters of Fe^{3+} ions substituted within the kaolinite structure (Schroeder and Pruett, 1996), and nano-particles of iron oxy-hydroxides or oxides (Malengreau *et al.,* 1994). Mössbauer spectroscopy provides additional data for Fe^{2+} ions in some of the kaolinites investigated here (FU7, KGa-1, GB3, and DCV samples; Bonnin *et al.,* 1982; Murad and Wagner, 1991, Delineau, 1994). The corresponding Fe^{2+} concentrations range within 25–50% of the total iron concentration (Table 1). The $[Fe^{3+}]_{EPR}$ values are significantly lower than the Fe^{3+} concentrations calculated from the Mössbauer data. A substantial part of Fe^{3+} is thus segregated into small oxy-hydroxide phases or concentrated in clusters within the kaolinite structure.

No clear relationship was found between the paramagnetic structural Fe^{3+} concentration and the concentration of stacking defects of kaolinite. This indicates that the structural modifications linked to dilute structural iron do not have a strong influence on the formation of stacking faults. Such observation is in agreement with those of Brindley *et al.* (1986). In addition, further investigations are needed to identify the other iron phases or clusters in kaolinite to obtain a better understanding of the relation between iron incorporation in kaolinite and specific geochemical parameters prevailing during crystal growth.

ACKNOWLEDGMENTS

The authors are indebted to M. Ebert for her reading of the manuscript. We thank P. Schroeder, S. Rice, J. Elzea Kogel, and S. Guggenheim for helpful and constructive reviews and comments. This work was supported by the CNRS/INSU program "Géomatériaux". This is contribution INSU-225 and IPGP-1646.

REFERENCES

Allard, T., Muller, J.-P., Dran, J.-C., and Menager, M.-T. (1994) Radiation-induced paramagnetic defects in natural kaolinites: Alpha dosimetry with ion beam irradiation. *Physics and Chemistry of Minerals,* **21,** 85–96.

Balan, E., Allard, T., Boizot, B., Morin, G., and Muller, J.-P. (1999) Structural Fe^{3+} in natural kaolinites: New insights from electron paramagnetic resonance spectra fitting at X and Q-band frequencies. *Clays and Clay Minerals,* **47,** 605–616.

Bogle, G.S. and Symmons, H.F. (1959) Paramagnetic resonance of Fe^{3+} in sapphyre at low temperatures. *Proceedings of the Physical Society,* **73,** 531–532.

Boizot, B. (1996) Cristallochimie des éléments de transition fer, chrome et manganèse dans les alumines techniques, Thèse, Université Pierre et Marie Curie, Paris, France, 196 pp.

Bonnin, D., Muller S., and Calas, G. (1982) Le fer dans les kaolins. Etude par spectrométries RPE, Mossbauer, EXAFS. *Bulletin de Minéralogie,* **105,** 467–475.

Brindley, G.W., Kao, C.-C., Harrison, J.L., Lipsicas, M., and Raythatha, R. (1986) Relation between structural disorder and other characteristics of kaolinites and dickites. *Clays and Clay Minerals,* **34,** 239–249.

Calas, G. (1988) Electron paramagnetic resonance. In *Spectroscopic Methods in Mineralogy and Geology, Volume 18, Reviews in Mineralogy,* F.C. Hawthorne, ed., Mineralogical Society of America, Chelsea, Michigan, 513–571.

Cases, J.-M., Liétard, O., Yvon, J., and Delon, J-F. (1982) Etude des propriétés cristallochimiques, morphologiques, superficielles de kaolinites désordonnées. *Bulletin de Minéralogie,* **105,** 439–455.

De Biasi, R.S. and Rodrigues, D.C.S. (1983) Influence of iron concentration and particle size on the ESR linewidth of Al_2O_3:Fe^{3+} powders. *Journal of Material Science Letter,* **2,** 210–212.

Delineau, T. (1994) Les argiles kaoliniques du Bassin des Charentes (France): Analyses typologique, cristallo-chimique, spéciation du fer et applications. Thèse, Institut National Polytechnique de Lorraine, Nancy, France, 627 pp.

Delineau, T., Allard, T., Muller, J-P., Barres, O., Yvon, J., and Cases, J.-M. (1994) FTIR reflectance *vs.* EPR studies of structural iron in kaolinites. *Clays and Clay Minerals,* **42,** 308–320.

Gaite, J-M., Ermakoff, P., and Muller, J-P. (1993) Characterization and origin of two Fe^{3+} EPR spectra in kaolinite. *Physics and Chemistry of Minerals,* **20,** 242–247.

Gaite, J-M., Ermakoff, P., Allard, Th., and Muller, J-P. (1997) Paramagnetic Fe^{3+}: A sensitive probe for disorder in kaolinite. *Clays and Clay Minerals,* **45,** 496–505.

Giese, R.F., Jr (1988) Kaolin minerals: Structures and stabilities. In *Hydrous Phyllosilicates (Exclusive of Micas), Volume 19, Reviews in Mineralogy,* S.W. Bailey, ed., Mineralogical Society of America, Chelsea, Michigan, 29–66.

Goodman, B.A. and Hall, P.L. (1994) Electron paramagnetic spectroscopy. In *Clay Mineralogy: Spectroscopic and Chemical Determinative Methods,* M.J. Wilson, ed., Chapman and Hall, London, 173–225.

Hall, P.L. (1980) The application of electron spin resonance spectroscopy to studies of clay minerals: I. Isomorphous substitutions and external surface properties. *Clay Minerals,* **15,** 321–335.

Lucas, Y., Chauvel, A., and Ambrosi, J.P. (1987) Processes of aluminium and iron accumulation in latosols developed on quartz rich sediments from central Amazonia (Manaus, Brazil). In *Proceedings of the International Meeting on Geochemistry of the Earth Surface and Processes of Mineral Formation, Granada, Spain,* R. Rodriguez-Clemente and Y. Tardy, eds., Consejo Superior de Investigaciones Cientificas, Madrid, 289–299.

Malengreau, N., Muller, J.-P., and Calas, G. (1994) Fe-speciation in kaolins: A diffuse reflectance study. *Clays and Clay Minerals,* **42,** 137–147.

Mehra, O.P. and Jackson, M.L. (1960) Fe oxide removal from soil and clays by a dithionite-citrate system buffered with sodium carbonate. *Clays and Clay Minerals,* **7,** 317–327.

Morin, G. and Bonnin, D. (1999) Modeling EPR powder spectra using numerical digonalization of the spin Hamiltonian. *Journal of Magnetic Resonance,* **136,** 176–199.

Muller, J.P. and Bocquier, G. (1987) Textural and Mineralogical relationships between ferruginous nodules and surrounding clayey matrices in a laterite from Cameroon. In *Proceedings of the International Clay Conference, Denver, 1985,* L.G. Schultz, H. van Olphen, and F.A. Mumpton, eds., The Clay Minerals Society, Bloomington, Indiana, 186–196.

Muller, J.P. and Calas, G. (1989) Tracing kaolinites through their defect centers. Kaolinite paragenesis in a laterite (Cameroon). *Economic Geology,* **84,** 694–707.

Muller, J.P. and Calas, G. (1993) Genetic significance of paramagnetic centers in kaolinites. In *Kaolin Genesis and Utilization,* H.H. Murray, W. Bundy, and C. Harvey, eds., The Clay Minerals Society, Boulder, Colorado, 261–289.

Muller, J-P., Manceau, A., Calas, G., Allard, T., Ildefonse, P., and Hazemann, J-L. (1995) Crystal-chemistry of kaolinite and Fe-Mn oxides: Relation with formation conditions of low-temperature systems. *American Journal of Science,* **295,** 1115–1155.

Murad, E. and Wagner, U. (1991) Mössbauer spectra of kaolinite, halloysite and the firing products of kaolinite: New results and a reappraisal of published work. *Neues Jahrbuch für Mineralogie Abteilung,* **162,** 281–309.

Olhoeft, G.R. (1981) Electrical properties of rocks. In *Physical Properties of Rocks and Minerals.,* Y.S. Touloukian, ed., MacGraw Hill, London, 257–330.

Petit, S. and Decarreau, A. (1990) Hydrothermal (200°C) synthesis and crystal chemistry of iron rich kaolinites. *Clay Minerals,* **25,** 181–196.

Schroeder, P.A. and Pruett, R.J. (1996) Fe ordering in kaolinites: Insights from ^{29}Si and ^{27}Al MAS NMR spectroscopy. *American Mineralogist,* **81,** 26–38.

Schroeder, P.A., Pruett, R.J., and Hurst, V.J. (1998) Effects of secondary iron phases on kaolinite ^{27}Al MAS NMR spectra. *Clays and Clay Minerals,* **46,** 429–435.

Shannon, R.D. and Rossman, G.R. (1992) Dielectric constants of silicate garnets and the oxide additivity rule. *American Mineralogist,* **77,** 94–100.

van Olphen, H. and Fripiat, J.J. (1979) *Data Handbook for Clay Materials and Other Non-Metallic Minerals.* Pergamon Press, Oxford, New York, 346 pp.

Weil, J.A., Wertz, J.E., and Bolton, J.R. (1994) *Electron Spin Resonance. Elementary Theory and Practical Applications.* Chapman and Hall, New York, 568 pp.

E-mail of corresponding author: balan@lmcp.jussieu.fr

(Received 4 August 1999; accepted 6 April 2000; Ms. 370; A.E. Jessica Elzea Kogel)